

<https://doi.org/10.1038/s42003-024-07369-x>

IGF-1 c.258 A > G synonymous mutation ameliorates senile osteoporosis



Zhaoguo Wang^{1,4}, Dayou Dai^{2,4}, Siyao Wang¹, Libo Zhang¹, Yi Li¹, Xunming Zhang¹, Yunyun Cheng^{1,3} & Linlin Hao¹

Senile osteoporosis (SOP) is a multifactorial, age-related progressive phenomenon with a considerable morbidity and mortality. IGF-1 is an important regulator of bone reconstruction and metabolism throughout life. Nevertheless, our previous study unexpectedly found there is no change in the peak bone mass with a altered IGF-1 gene expression led by IGF-1 c.258 A > G synonymous mutation. Considering its involvement in the cellular senescence, we suspected c.258 A > G may participate in SOP. Therefore, the effect of IGF-1 c.258 A > G on SOP was firstly detected, the changes of bone formation and bone resorption index in SOP mice with two genotypes indicated it improved SOP. Then, the in vitro study confirmed the mutation ameliorates SOP by promoting the growth and development of senescent osteoblasts. At last, co-culture of osteoblast and osteoclast further verified the mutation prevents SOP by increasing the bone formation capacity of senescent osteoblasts. Collectively, this study illuminated the role of IGF-1 c.258 A > G in ameliorating SOP.

Senile osteoporosis (SOP) is an important public health problem associated with the increased aging population worldwide and is considered primary osteoporosis characterized by reduced bone mineral density (BMD) and hip fractures caused by deteriorated bone tissues, leading to pain of the patient and high socioeconomic costs^{1–3}. Prior studies indicated that SOP is caused by a dysregulation of bone remodeling between osteoclasts and osteoblasts in the elderly, with decreased osteoblast activity accompanied by increased osteoclast activity^{4,5}. Therefore, with the growing burden of SOP, it is significant to find novel targets and effective treatments for this disease.

Substantial evidence indicated that insulin-like growth factor-1 (IGF-1) is important for bone growth and maintenance through their direct or indirect actions on osteoblast^{6–8}. Conditional knockout of *IGF-1* mice reduces osteoblast number and activity^{9–11}, and its overexpression enhanced the osteogenic ability to aged bone marrow mesenchymal stem cells¹². A meta-analysis further elaborated a decisive association between IGF-1 and SOP in the elderly. During aging, decreased serum IGF-1 levels and local expression of IGF-1 in bone were found to be associated with a decrease in BMD¹³. Interestingly, our group previously identified only one synonymous mutation c.258 G > A (rs322131043) in the coding region of the pig *IGF-1* gene¹⁴, which is highly conserved among species¹⁵, including humans (rs766050142), and found that there is no change in the peak bone mass with a altered *IGF-1* gene expression led by this synonymous mutation¹⁶. Considering IGF-1 involved in the cellular senescence process, we suspected the c.258 G > A synonymous mutation

may be involved in SOP by affecting IGF-1 expression considering the relationship between the IGF-1 level and SOP.

Given that most of the current basic research on synonymous mutations stay at the cellular level, few examples of animal experiments have been used to validate the contribution of synonymous mutations to biological phenomena or to attempt a comprehensive assessment of the effects of these mutations. Here, this study illuminated whether and how the *IGF-1* c.258 A > G ameliorate SOP, which may be hopeful to produce a more efficient IGF-1 analogue against SOP.

Results

The frequency of IGF-1 c.258 A > G distribution and incidence of osteoporosis

Considering the only one synonymous mutation c.258 G > A (rs322131043) in the coding region of the pig *IGF-1* gene¹⁴ is highly conserved among species¹⁵, including human (rs766050142), and the conjecture it may be involved in SOP, this study aimed to explore whether IGF-1 c.258 A > G is involved in the development of SOP. We firstly analyzed the incidence distribution of the SOP worldwide (Fig. 1a) and learned the frequency of IGF-1 c.258 A > G was significantly different in various people, and the frequency of codon GCA (the mutation located) encoded Ala is higher in South Asia and Africa than in Finnish and Non-Finnish European using the database data (<http://asia.ensembl.org/rs766050142> (SNP)-Explore this variant - Homo_sapiens - Ensembl genome browser 112)

¹College of Animal Science, Jilin University, Changchun, Jilin, China. ²State Key Laboratory of Systems Medicine for Cancer, Shanghai Cancer Institute, Ren Ji Hospital, School of medicine, Shanghai Jiao Tong University, Shanghai, China. ³NHC Key Laboratory of Radiobiology, College of Public Health, Jilin University, Changchun, Jilin, China. ⁴These authors contributed equally: Zhaoguo Wang, Dayou Dai. e-mail: chengyy@jlu.edu.cn; haolinyin@jlu.edu.cn

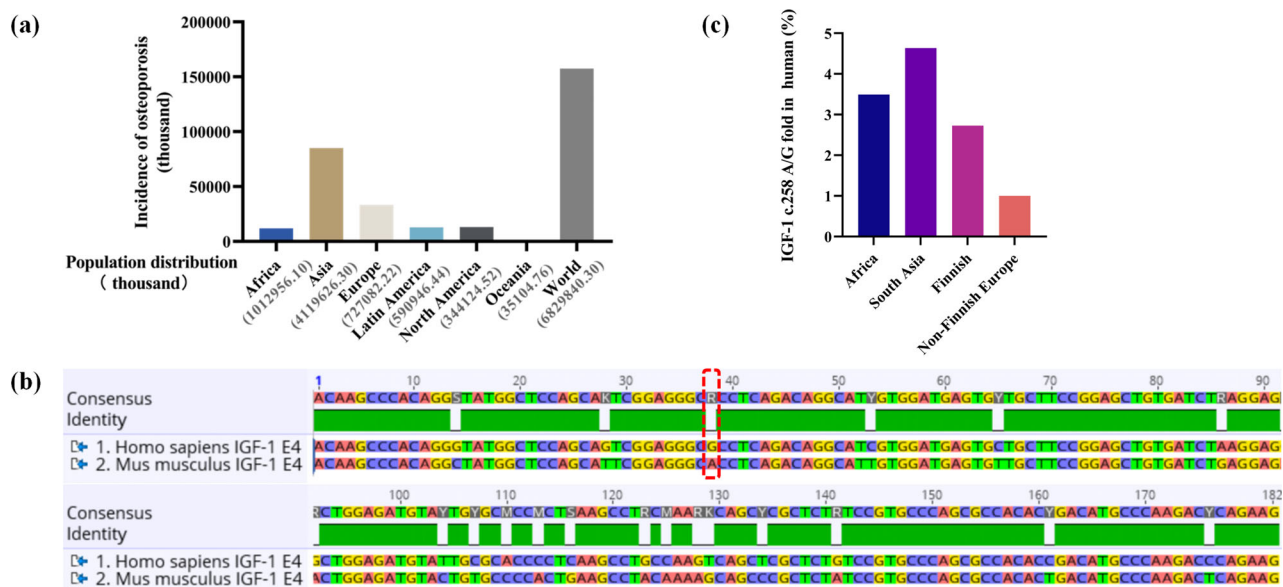


Fig. 1 | The frequency of *IGF-1* c.258 A > G distribution and incidence of osteoporosis. a The incidence of osteoporosis in individuals aged over 50 years. **b** Homology alignments of *IGF-1* exon 4 in human and *Mus musculus*, the red dotted

box referred to the synonymous mutation site of c.258 A > G. **c** Human *IGF-1* c.258 A/G folding in different regions and countries.

(Fig. 1c). Furthermore, the mice model were used to detect the effect of this locus on SOP because of the 89.0% identity of the homology of *IGF-1* in human and mice containing the synonymous mutation c.258 A > G (Fig. 1b).

Construction and identification of different genotypes of mice SOP model

The overall flow for the construction of SOP is shown in Fig. 2a. There were no significant differences in body weight, tibial length and weight, visceral index and visceral histopathology between the two genotypes of mice at different stages of growth and development (Fig. 2b–j), indicating the *IGF-1* c.258 A > G synonymous mutation did not affect the normal growth and health of mice. To verify whether the SOP mouse model was successfully constructed and whether *IGF-1* c.258 A > G plays a key role in the resistance to oxidative stress in SOP, we measured the activities of SOD, CAT, GSH-PX and content of MDA in liver homogenates. SOP mice of both genotypes showed significantly lower SOD, CAT and GSH-PX activities ($P < 0.05$, $P < 0.01$, $P < 0.01$) and significantly higher MDA content ($P < 0.01$) compared to their corresponding controls (Fig. 2k–n). The above results indicated that D-Gal-induced SOP was successfully constructed in mice. However, in WT(AA) and Ho(GG) SOP groups, there was no significant difference in anti-oxidation index. The results showed that the *IGF-1* c.258 A > G did not play a significant role in D-Gal-induced resistance to oxidative stress in SOP.

IGF-1 c.258 A > G synonymous mutation increases the bone mass in SOP mice

To study the potential role of *IGF-1* c.258 A > G synonymous mutation in SOP, we firstly measured the circulating levels of *IGF-1* in WT(AA) SOP mice and found they were significantly lower than those of 8-week-old WT(AA) mice, while the Ho(GG) SOP mice successfully increased the serum levels (Fig. 3a). Micro-CT analysis showed the trabecular bone mass of mice reaches the peak at their sexually mature period (about 8-weeks-old) and declines sharply in the next few months. WT(AA) mice started to lose bone mass from then on, while Ho(GG) mice continued to accrue bone, with bone mass remaining stable until aged (Fig. 3b–h). Ho(GG) SOP mice displayed elevated BMD, vertebral bone volume (BV/TV), trabecular number (Tb.N), and reduced trabecular separation (Tb.Sp) and structural

model index (SMI) compared with WT(AA) SOP mice, while trabecular thickness (Tb.Th) was not changed between these two groups. In addition to trabecular measures of bone volume, cortical BV/TV and cortical thickness (Ct.Th) of Ho(GG) SOP mice also significantly increased than WT(AA) SOP mice ($P < 0.05$) (Fig. 3i–k).

Histomorphometric analyses confirmed the increased bone mass in Ho mice (Fig. 3l, m). Ho SOP mice displayed an increased number of osteoblasts (N.Ob) and bone area per total area (BA/TA) (Fig. 3n, o), and a decreased number of osteoclasts (N.Oc) and osteoclast surface per bone surface (Oc.S/BS), indicating a more active bone remodeling status (Fig. 3p, q).

IGF-1 c.258 A > G synonymous mutation promotes bone formation and suppresses bone resorption in SOP mice

As the increase in bone mass was developing with age, we investigated whether the *IGF-1* c.258 A > G affected *IGF-1* levels were time-dependent in bone. Results indicated 8-week-old Ho(GG) mice had significantly lower levels of *IGF-1* expression in bone tissue compared to 8-week-old WT(AA) mice, without a significant change of BMD, tibia weight and tibia length, the control groups of the two genotypes mice showed no difference in the expression level of *IGF-1* in bone tissue (Fig. 4a, b). However, Ho(GG) SOP mice showed significantly higher *IGF-1* level than that of WT(AA) SOP mice.

Based on the changes of results in Micro-CT, the further analysis of marker genes in osteoblasts including ALP, OCN, OPN, COL-1, OSX, RUNX2 and in osteoclasts including TRAP and RANKL. ALP, OCN, OPN, COL-1, OSX, RUNX2 showed significantly increased expression levels in Ho(GG) SOP mice compared with the WT(AA) SOP mice (Fig. 4c, g). And TRAP and RANKL significantly decreased in Ho SOP mice, demonstrating that both osteoblast and osteoclast-associated genes are regulated in Ho(GG) SOP mice.

Considering that serum ALP, OPG, P1NP, RANKL and CTX-1 are the most important markers of bone turnover used to assess bone formation and resorption^{17–19}. With aging, these serum biochemical markers exhibited a decrease level of serum ALP, CTX-1 and P1NP, while while in the SOP group, Ho (GG) mice showed a relatively high expression level of P1NP and a low expression of CTX-1 than in WT(AA) mice (Fig. 4h–j). Moreover, we detected a significantly higher OPG/RANKL ratio in Ho(GG) SOP mice

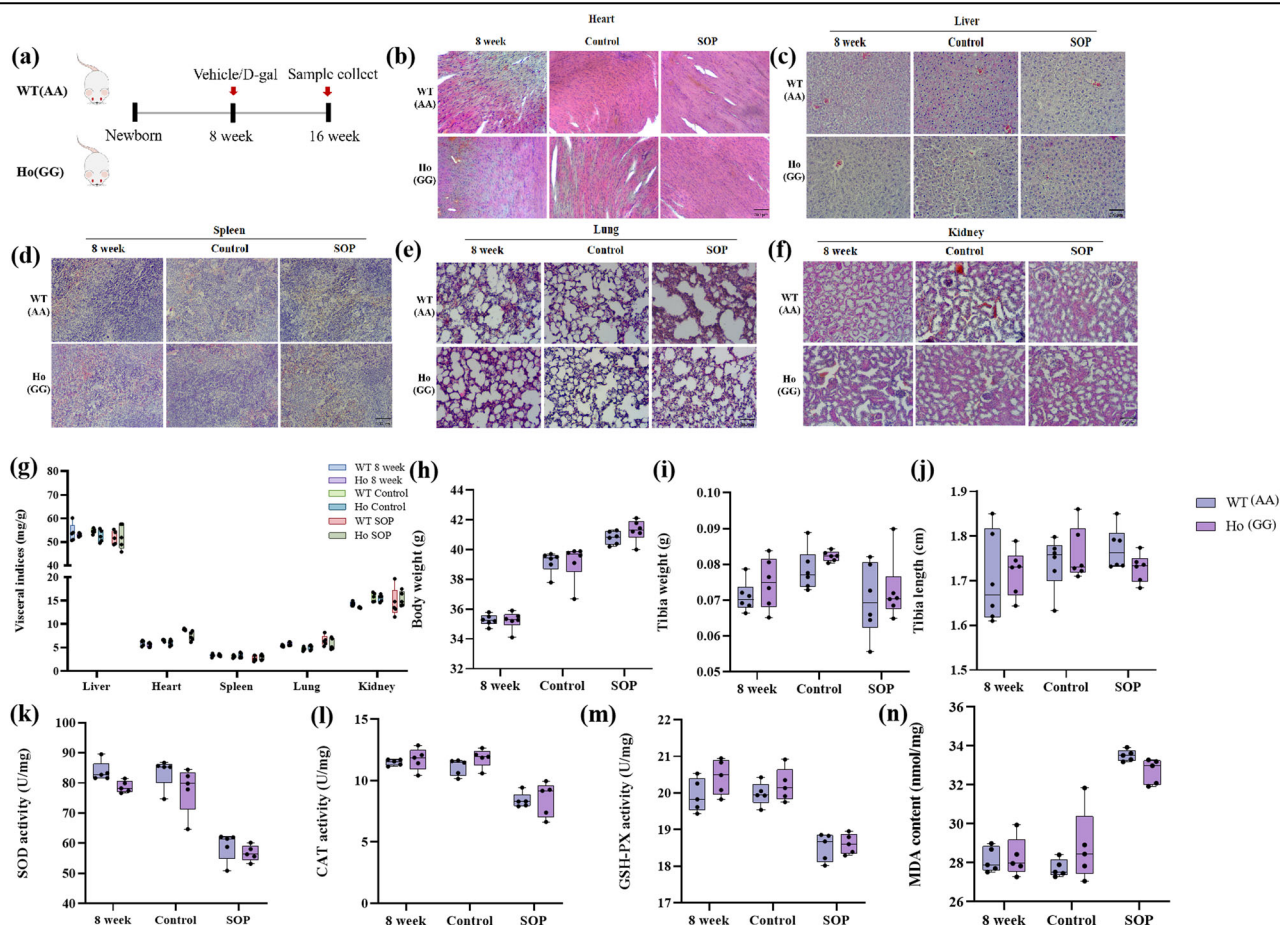


Fig. 2 | Construction and identification of different genotypes of mice
SOP model. **a** Schematic illustration of the D-gal-induced bone loss experiment performed in 8-week-old WT(AA) and Ho mice. **b–f** Effect of D-gal on cell morphology of liver, heart, spleen, lung and kidney tissues (H&E staining, scale bar 200 μ m, magnification 40 \times) at different developmental stages. **g** Visceral index of

different viscus in different genotypes mice at different developmental stages. **h–j** Body weight, tibia weight, and tibia length of mice of different genotypes at different developmental stages. **k–n** Effect of D-gal on related antioxidant indices in different genotypes mice (the activity of SOD, CAT, GSH-PX, and MDA). The results are presented as mean \pm SD ($n = 5$), * $P < 0.05$; ** $P < 0.01$.

compared with WT(AA) SOP mice, which was primarily driven by increased levels of OPG in Ho(GG) SOP mice compared with WT(AA) SOP mice (Fig. 4k–m). Considering the OPG/RANKL ratio and positive role of P1NP in osteoblast activity, as well as the positive role of CTX-1 in osteoclast activity, we concluded the Ho (GG) SOP mice have a relative higher bone formation ability.

IGF-1 c.258 A > G synonymous mutation promotes proliferation, migration, and osteogenesis of H_2O_2 -induced CNCCs and MC3T3-E1 cells

This study successfully obtained two genotypes of CNCCs (Supplementary Fig. 1a, b). As the aging of CNCCs are accompanied with deterioration of proliferation, differentiation, mineralization and migration activity, we evaluate sought to the effect of IGF-1 c.258 A > G synonymous mutation on osteogenic proliferation, differentiation, mineralization and migration of H_2O_2 -induced CNCCs in vitro. CNCCs H_2O_2 -induced model was successfully constructed (Fig. 5a–c). Based on previous studies, IGF-1 can strongly induce osteogenic proliferation and migration in H_2O_2 -induced CNCCs. To confirm this, higher CNCC-IGF-G expression level was detected compared to CNCC-IGF-A (Fig. 5d, e) and then cell proliferation was compared between two genotypes cells in the culture medium for 1, 2, 3, 4, and 5 days, which was determined by CCK-8 and EdU assay (Fig. 5f–i). We found that CNCC-IGF-G cells were enough to increase the ability of cell proliferation in a time-dependent manner, and IGF-1 c.258 A > G synonymous mutation dramatically elevated cell proliferation of H_2O_2 -induced CNCC. We investigated the migration of CNCC-IGF-A and CNCC-IGF-G

cells through scratch assay. At 9 and 18 h after scratching, Fig. 5j, k presented that the H_2O_2 -induced CNCC-IGF-G cells showed an accelerated speed of migration. Next, we cultured CNCC-IGF-A and CNCC-IGF-G cells in osteogenic induction medium. As determined by the ALP and Alizarin Red S (ARS) staining, CNCC-IGF-G cells exhibited a stronger osteogenic potential than that of the controls (Fig. 5l–n). In addition, the expression of the osteogenic-related genes, such as ALP, OCN, OPN, COL-1, OSX, and RUNX2, was upregulated in CNCC-IGF-G cells (Fig. 5o).

Meanwhile, we used MC3T3-E1 cells to construct IGF-1 c.258 G > A synonymous mutation model by ABE edited system (Supplementary Fig. 1e–j) to further verify the effect of this locus on osteoblast proliferation, migration, and osteogenesis. Results also found that this synonymous mutation dramatically elevated cell proliferation, migration, and stronger osteogenic potential of H_2O_2 -induced MC3T3-E1 cells (Fig. 6a–o), which were consistent with the results conducted in CNCCs. In addition, IGF-1 stimulate growth and differentiation of osteoblasts may be modulated by their binding proteins (IGFBPs), so we further detected the effects of IGF-1 c.258 A > G on IGFBP3, IGFBP5 and the binding affinity differences of IGFBP-3 or IGFBP-5 with the IGF-1 of two genotypes, results indicated that the c.258 A > G did not altered the expression level of IGFBP3 and IGFBP5, as well as the binding affinity of IGFBP-3 or IGFBP-5 with IGF-1 (Fig. 5P).

IGF-1 c.258 A > G synonymous mutation promotes bone formation in an osteoblast-osteoclast co-culture system

Due to the mutual coupling between osteoblasts and osteoclasts, the individual effects of IGF-1 c.258 A > G synonymous mutation on osteoblasts

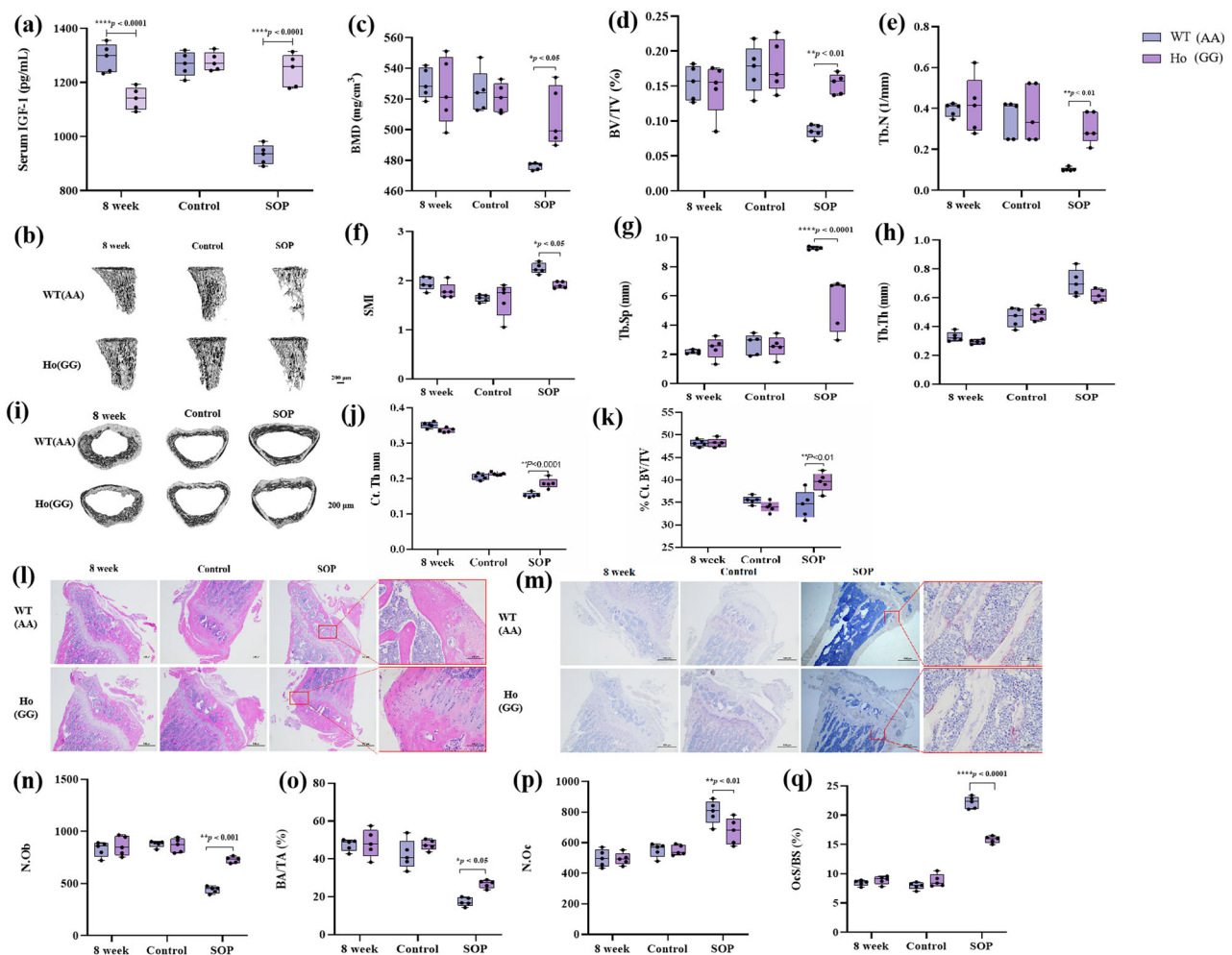


Fig. 3 | *IGF-1* c.258 A > G synonymous mutation improves bone loss in SOP. **a** Circulating IGF-1 levels in serum of different genotypes mice at different developmental stages using ELISA. **b** Representative micro-CT photographs of trabecular bones from tibial WT (AA) and Ho mice at different developmental stages (Scale bar 200 μ m, magnification 40 \times). **c** Quantitative micro-CT analyses of BMD of the proximal tibial metaphysis. **d-h** Three-dimensional reconstruction and quantitation of the indicated parameters of trabecular bone from the proximal tibial metaphysis of WT (AA) and Ho mice at different developmental stages, using micro-CT. **i** Representative images of cortical bone. **j, k** Bone morphometric analysis of the

indicated parameters of cortical bone at the diaphysis of the tibia, close to the site of the intersecting fibula using μ CT ($n \geq 4$). **l, m** H&E and TRAP staining of histological sections, obtained from the proximal tibial metaphysis of WT (AA) and Ho (GG) mice at different developmental stages, and representative images are shown (Scale bars 500 μ m, magnification 40 \times). **n-q** Histomorphometric analysis of H&E, TRAP-stained tibial sections, N.Ob, BV/TV, N.Oc, and OcS/BS of WT (AA) and Ho (GG) mice at different developmental stages ($n \geq 4$). The results are presented as mean \pm SD ($n = 5$). * $p < 0.05$; ** $p < 0.01$.

and osteoclasts alone may not reflect the real status of bone homeostasis in animals. Therefore, we first performed co-culture experiments on two genotypes of primary osteoblasts and primary osteoclasts (Supplementary Fig. 1c, d) using transwell chamber to simulate the in vivo microenvironment. Osteogenic and osteolytic activity of cells were detected by ARS and TRAP staining (Supplementary Fig. 2). Osteoblast genes OPG and ALP expression decreased in the co-culture system compared with the culture alone group, while RANKL expression increased compared with the culture alone group by qRT-PCR; osteoclast-related TRAP and NF- κ B gene expression decreased significantly compared with the culture alone group by qRT-PCR. In the co-culture system, *IGF-1* c.258 A > G synonymous mutation significantly up-regulated the protein expression of OPG in senescent osteoblasts, while RANKL protein expression did not change significantly and the OPG/RANKL ratio increased (Fig. 6). Subsequently, we established a two genotypes osteoblast-monogenic osteoclast (Supplementary Fig. 1k) co-culture system using transwell chambers to further investigate the effect of *IGF-1* c.258 A > G synonymous mutation on osteoblast activity and osteoclast differentiation, and received similar results.

Discussion

The current study confirmed the *IGF-1* c.258 A > G synonymous mutation has an ameliorative effect on SOP in aged mice, hopeful to produce a more efficient IGF-1 analogue against SOP. Human SOP is usually characterized by reduced bone mass and microstructural changes, mainly attributed to osteoblastic dysfunction, leading to a significantly increased risk of fracture and subsequent disability. One of the limitations of the investigation for SOP is the lack of physiologically relevant bone models of aging. So, building an animal model of SOP plays an important role in evaluating the pathogenesis, pathological changes, prevention and treatment measures, and new therapeutic drugs. At present, the most commonly used SOP animal models are rapid aging osteoporosis animal model²⁰, D-Gal induced SOP animal model²¹, and natural senescence SOP animal model²². In this study, the D-Gal induced SOP mice were constructed using eight-week-old male ICR mice through the injection of D-galactose at a dose of 400 mg/kg/day for 8 weeks to evaluate the effect of *IGF-1* c.258 A > G on SOP, which is a SOP model that are simple, low price, small side effects, high survival rate and high reproducible rate during the whole experimental period. And with

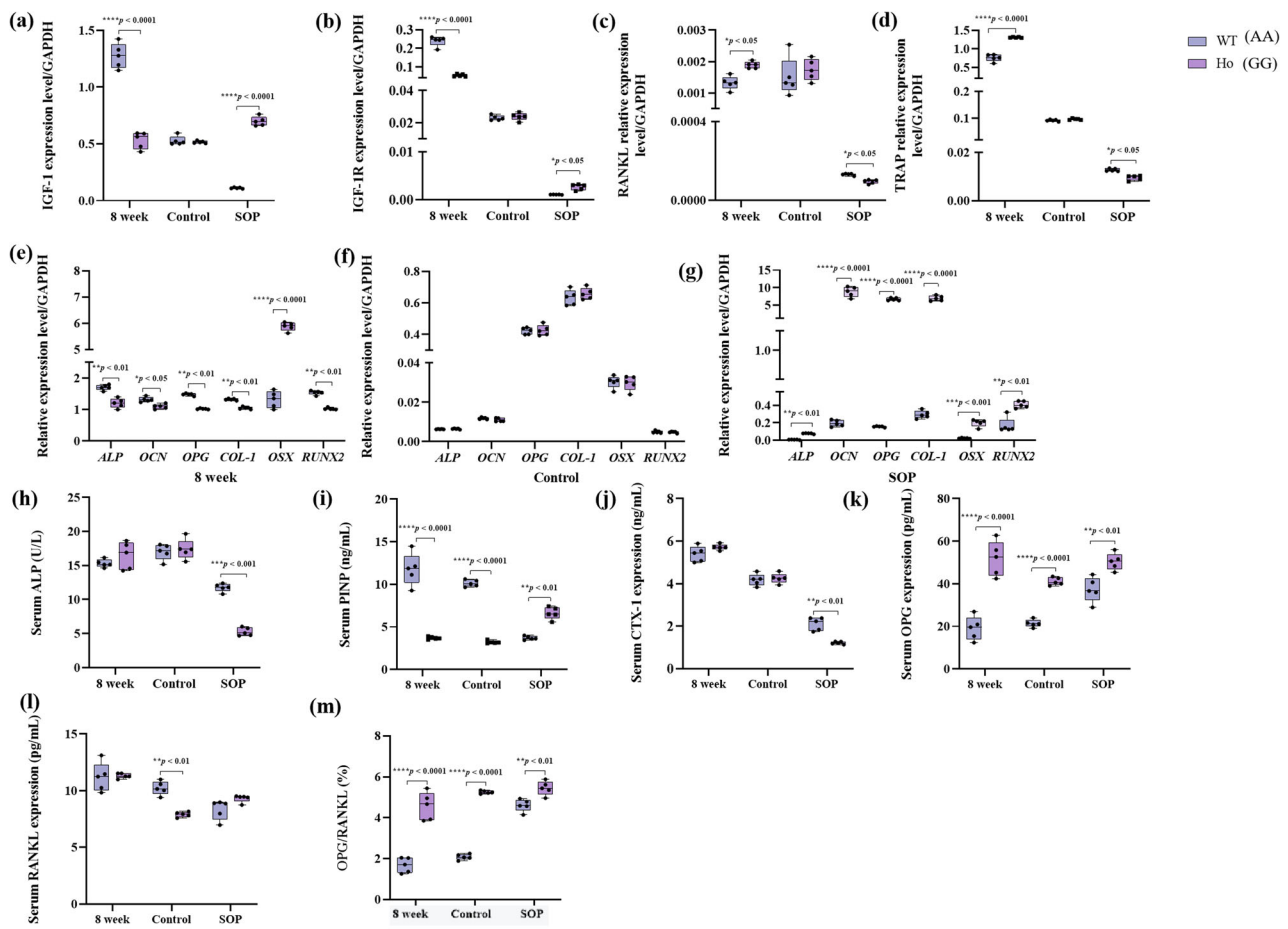


Fig. 4 | IGF-1 c.258 A > G synonymous mutation inhibits bone resorption and increases bone mass in SOP mice. **a, b** The expression level of IGF-1 and IGF-1R in the tibial bone of WT(AA) and Ho(GG) mice at different developmental stages by qRT-PCR. **c–g** The expression level of RANKL, TRAP, ALP, OCN, OPN, COL-1, OSX, and RUNX2 in tibial bone from different developmental stages WT(AA) and Ho(GG) mice was analyzed using qRT-PCR. **h–m** Levels of ALP, PINP, CTX-1, OPG, and RANKL were measured in

serum of different developmental stages of WT(AA) and Ho(GG) mice using ELISA. OPG, osteoprotegerin; PINP, procollagen type 1 N-terminal propeptide; CTX C-terminal telopeptide of type I collagen, RANKL receptor activator of NF- κ B ligand. All data shown were obtained from male mice. The results are presented as mean \pm SD ($n = 5$). * $P < 0.05$; ** $P < 0.01$; *** $P < 0.001$.

aging, WT mice exhibited significantly decreased BMD, BV/TV, Tb.N, N.Ob and increased Tb.Sp, Tb.Th, N.Oc, suggesting the appearance of similar changes in human SOP, although it is not a model of natural aging. At present, bisphosphonates and recombinant human parathyroid hormone (rhPTH) are the two drugs approved by the FDA/EMA for the treatment of SOP²³, while the side effects, such as osteosarcoma and osteonecrosis limited their use in long-term treatment^{24,25}. IGF-1 may be an ideal therapeutic drug because it is one of the most abundant substances in the bone matrix, secreted locally, circulates systemically, and functionally related to the BMD^{6,26}. The IGF-1 c.258 A > G may produce a more efficient IGF-1 analogue according to the reports that indicated genetic factors played an important role in the pathogenesis of SOP^{27–29}, for instance, OPG g.27563 G > A is associated with lower BMD values and increased risk of SOP³⁰, and CD44 G > A synonymous mutation might be increasing susceptibility to osteoporosis³¹. Our experimental results confirmed that Ho(GG) mice have more IGF-1 level than that in WT(AA) mice in the aging stage, which led us to affirm that c.258 A > G has a potential role in SOP. Study also indicated IGF-1 stimulate growth and differentiation of osteoblasts, and these biological functions can be modulated by their binding proteins (IGFBPs), in which the IGFBP-4 and -5 are the most abundant IGFBPs produced by osteoblasts³² and the IGFBP-3 is the most abundant IGF-binding protein in postnatal blood³³, unfortunately, in this study, c.258 A > G did not altered the binding affinity of IGFBP-3 or IGFBP-5 with IGF-1, which may be due to c.258 A > G is not located in the critical region

on the IGF-1 gene for binding to IGFBPs. This also reminds us of our previous study in which c.258 A > G altered its relative binding affinity to the receptor IGF-1R, because it located in the critical region of IGF-1 binding to IGF-1R¹⁴.

In addition, study has proposed the GH/IGF-1 plays a critical role in glucocorticoid-induced osteoporosis³⁴ and another study indicated that IGF-1 reversed the glucocorticoid-induced osteoporosis by osteogenic inhibitory effect of dexamethasone via PI3K/AKT pathway³⁵, indicating the positive relationship between IGF-1 expression level and improvement of secondary osteoporosis. We speculated that IGF-1 c.258 A > G also has an effect on secondary osteoporosis based on the IGF-1 c.258 A > G changes IGF-1 expression. Therefore, how the c.258 A > G involved in the SOP is the main issue we are concerned in this study.

Currently, the bone loss and bone pathological changes are the important reference indicators for the evaluation of SOP³⁶. The index of bone loss including BMD, BV/TV, SMI, Tb. N, Tb. Th and Tb. Sp³⁷ and the performance of bone pathological including the decrease of N. Ob, BA/TA and the increase of N.Oc, Oc.S/BS³⁸. Our results indicated the role of IGF-1 c.258 A > G in improving SOP. In terms of the marker genes of bone turnover in SOP, abnormally high levels of CTX-1 (specific indicator of bone resorption) and abnormally low levels of PINP (marker of bone formation) can be detected¹⁸. In addition, loaded osteocytes can produce signaling molecules, such as Wnts, OPG and RANKL, which modulate the recruitment, differentiation, and activity of osteoblasts and osteoclasts³⁹.

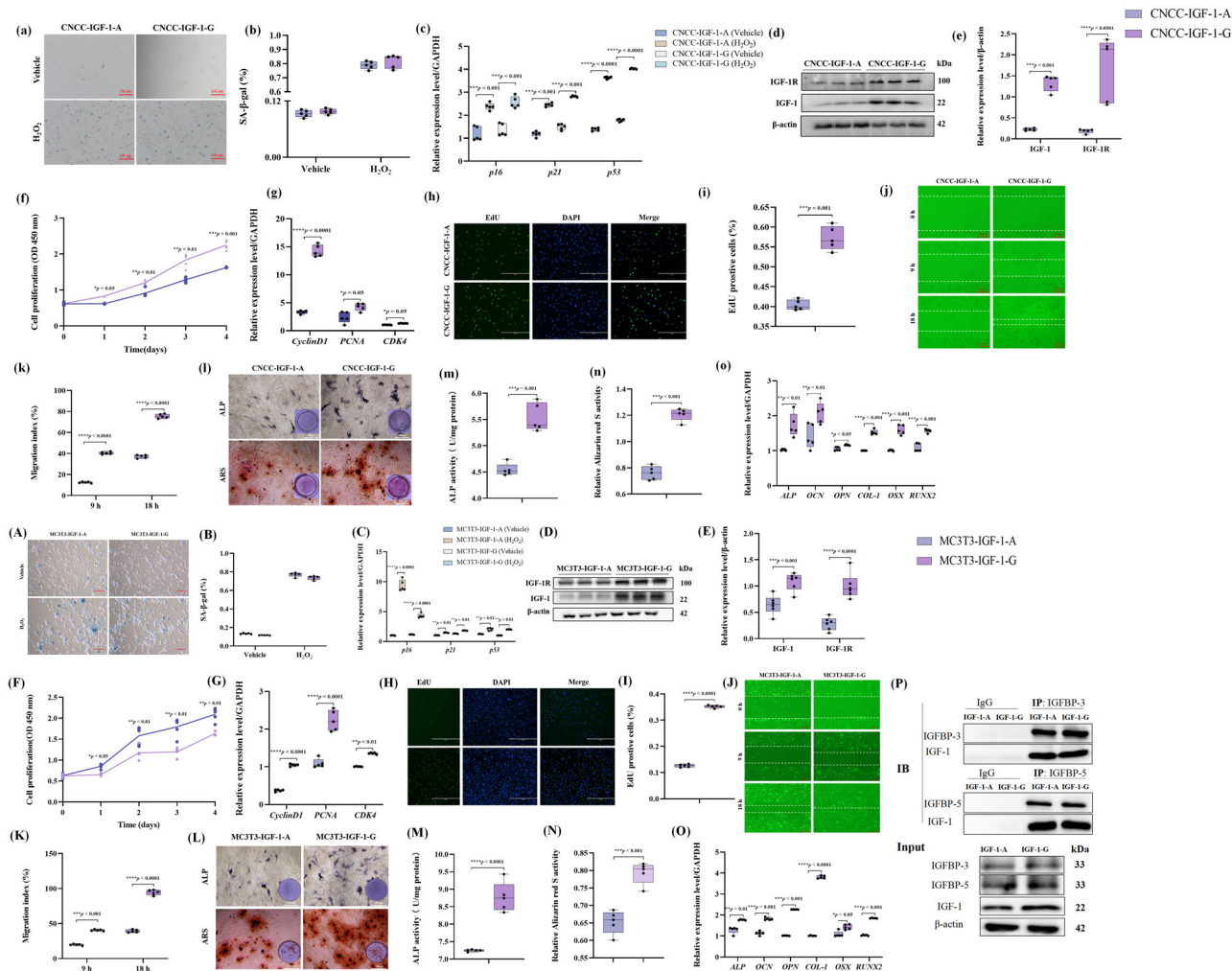


Fig. 5 | IGF-1 c.258 A > G synonymous mutation promotes the proliferation, migration, and mineralization of H₂O₂-induced CNCC cells and MC3T3-E1 cells. a SA-β-gal staining of CNCC-IGF-1-A and CNCC-IGF-1-G cells stimulated with H₂O₂. Scale bar 100 μm. **b** Quantification of SA-β-gal positive CNCC-IGF-1-A and CNCC-IGF-1-G cells. **c** The expression level of senescence-associated genes (*p16*, *p21*, and *p53*) in H₂O₂-induced CNCC-IGF-1-A and CNCC-IGF-1-G cells using qPCR. **d, e** The expression level of IGF-1 and IGF-1R detected by western blot. **f** CCK-8 assay of the proliferation of H₂O₂-induced cells of different genotypes at 0, 1, 2, 3, and 4 days. **g** The expression level of cell proliferation-related genes (*CyclinD1*, *PCNA*, and *CDK4*) in H₂O₂-induced different genotypes cells by qRT-PCR. **h** EdU incorporation in aged different genotypes cells. Scale bar 200 μm. **i** Statistical results of EdU staining, CNCC-IGF-1-G cells increased the number of

EdU cells. **j, k** Scratch assay of H₂O₂-induced different genotypes cells and quantitative analysis. White dashed lines indicate the start (0 h), half (9 h), and end (18 h) positions of different genotypes cells after scraping. Scale bar 50 μm.

l Representative images of ALP and ARS staining of H₂O₂-induced different genotypes cells. **m** Quantitative analysis of the ALP activity in H₂O₂-induced different genotypes cells. **n** Quantitative analysis of the mineralization in H₂O₂-induced different genotypes cells using 10% cetylpyridinium chloride. **o** Quantitative qRT-PCR results of mRNA expression of *ALP*, *OCN*, *OPN*, *COL-1*, *OSX*, and *RUNX2* in aged different genotypes cells. **A–O** Results in MC3T3-E1 cells corresponding to (a–o). **P** Binding affinity detection of IGFBP-3 or IGFBP-5 with the IGF-1 of two genotypes in the MC3T3-E1 cells. The results are presented as mean ± SD (*n* = 5). **P* < 0.05; ***P* < 0.01; ****P* < 0.001.

RANKL can promote bone resorption through stimulating the proliferation and differentiation of osteoclasts by combining with RANK expressed in osteoclasts. OPG, mainly derived from osteoblasts, has an inhibitory effect on bone resorption by competitively combining with RANKL, that is osteoblasts can indirectly control osteoclast differentiation and thereby prevent excessive osteoclast-mediated bone loss by regulating the ratio of RANKL to OPG. And studies have indicated that the differentiation, proliferation, maturation of osteoblasts can improve bone density and bone metabolism in bone osteoporosis fracture rats^{40–42}. Therefore, significantly lower levels of CTX-1 and significantly higher PINP, OPG, and OPG/RANKL levels in Ho(GG) SOP mice indicating IGF-1 c.258 A > G promotes bone formation and suppresses bone resorption in aged mice. Moreover, treatment of osteoblasts IGF-1R inhibitor significantly inhibited the increase in RANKL/OPG ratio by IGF-1⁴⁰, suggesting that the difference of c.258 A > G on osteoblasts development may be caused by the effect on OPG/RANKL through IGF-1 binding difference with IGF-1R.

The role of osteoblasts is crucial in the process of bone reconstruction, and changes in their number and function are directly related to the development of SOP. Therefore, stimulation of osteoblast proliferation, differentiation and mineralization. The results of IGF-1 c.258 A > G promoting the proliferation of osteoblasts, increasing the ALP activity of osteoblasts indicated c.258 A > G have the positive role in bone formation and the improvement of SOP. Bone resorption of the osteoclasts is also closely related to SOP. Unexpectedly, we did not found the mutation altered osteoclast proliferation, differentiation, or bone resorption. Yet, the osteoblasts and osteoclasts cultured alone may not reflect the real situation of bone metabolism in animals. Therefore, in this part, we established an osteoblast-osteoclast co-culture system with the two genotypes for both cell types and a two genotype osteoblast-monogenic osteoclast co-culture system, confirming this synonymous mutation promoted osteoblast activity and bone formation while not affect osteoclast differentiation, suggesting that IGF-1 c.258 A > G does not affect bone resorption by senescent

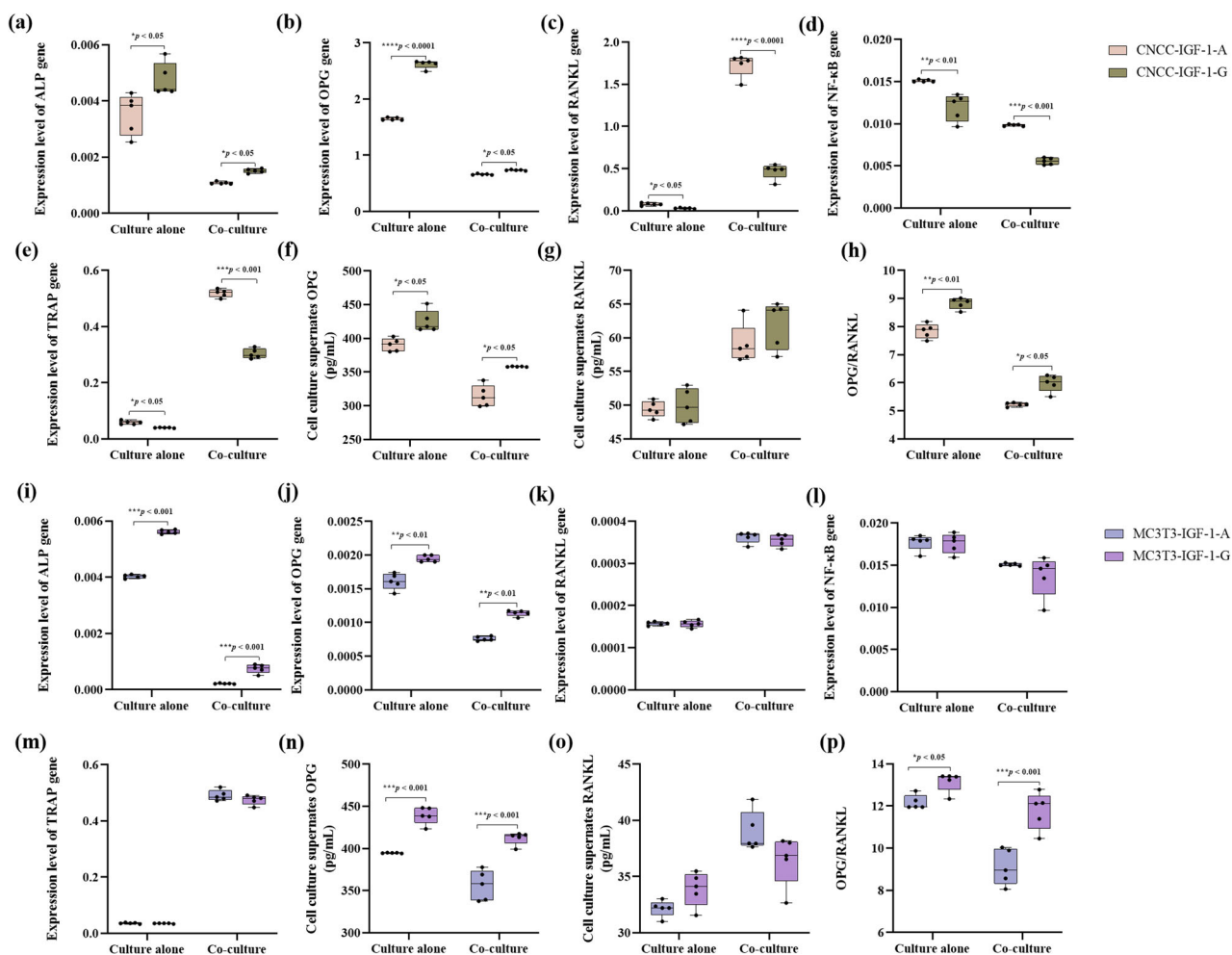


Fig. 6 | *IGF-1* c.258 A > G synonymous mutation promotes bone formation in an osteoblast-osteoclast co-culture system. **a–e** The expression level of osteogenesis and osteoclast-related genes in H_2O_2 -induced primary osteoblasts and osteoclast with two genotypes in co-culture by qRT-PCR. **f–h** The expression level of OPG and RANKL in aged primary osteoblasts and osteoclast with two genotypes in culture

alone and co-culture by ELISA. **i–m** The expression level of osteogenesis and osteoclast-related genes in aged MC3T3-E1 with two genotypes and RAW264.7 in co-culture by qRT-PCR. **n–p** The expression level of OPG and RANKL in aged MC3T3-E1 with two genotypes and RAW264.7 in co-culture by ELISA. The results are presented as mean \pm SD ($n = 5$). * $p < 0.05$; ** $p < 0.01$; *** $p < 0.001$.

osteoclasts, but prevents senescence-induced bone loss by increasing the bone formation capacity of senescent osteoblasts.

In conclusion, we demonstrate that *IGF-1* c.258 A > G synonymous mutation improves SOP by rejuvenating the senescent osteoblasts, which has the potential to produce a more effective drug for SOP.

Materials and methods

Animals and ethics statement

Wild-type (WT) and homozygous (Ho) ICR male mice were obtained from Liaoning Changsheng Experimental Animal Center (Liaoning, China) and generated as previously described¹⁶, respectively. Mice were housed in cages at a constant temperature of $23 \pm 1^\circ\text{C}$, with a 12-h light/dark cycle and $55 \pm 5\%$ humidity under specific pathogen-free conditions, with free access to water and diet. All animal experiments were supervised and reviewed by the Animal Welfare and Research Ethics Committee and the Laboratory Animal Center of Jilin University (SYXK [Ji] 2016–0001).

Senile osteoporosis model construction experimental protocol

Thirty 8-week-old Ho(GG) mice and thirty age-matched male WT(AA) mice were randomly allocated into six groups with ten mice per group, including the 8-week-old WT mice (sacrificed), the 8-week-old Ho(GG)

mice (sacrificed), the WT(AA) control group (2% ethanol in saline + saline), the Ho(GG) control group (2% ethanol in saline + saline), the WT(AA) SOP group (2% ethanol in saline + 400 mg/kg D-gal), and the Ho(GG) SOP group (2% ethanol in saline + 400 mg/kg D-gal). The mice in the control group were administered normal saline, and the remaining mice were injected subcutaneously with D-gal at a dose of 400 mg/kg/d for 58 days. After 58 days subcutaneous injection and to allow the onset of osteoporosis, all mice were sacrificed. Bone loss in the tibiae of these mice was assessed by micro-CT and histological analysis.

Micro-CT analysis

The right proximal tibia was dissected and fixed for 24 h in 4% paraformaldehyde and then kept in 70% ethanol at 4°C before being prepared for micro-CT analysis. As previously described³⁷, the metaphyseal trabecular bone and cortical bone was scanned using viva CT50 (Scanco Medical) in a spatial resolution of $8\ \mu\text{m}$ (55 KVP, $114\ \mu\text{A}$, integration time 500 ms). Then, three-dimensional morphometric analysis was performed by the NRecon, CTvox, Data Viewer, and CTAn software. The region of interest was the proximal tibial growth plate and the proximal tibial metaphysis located between 0 and 2 mm distal to the growth plate epiphyseal junction.

Histomorphometry analysis

Histomorphometry analysis of mouse left tibia from WT(AA) and Ho(GG) was analyzed as described³⁸. In brief, the left tibia was dissected from soft tissue, fixed with 4% paraformaldehyde, decalcified in 10% EDTA buffer, embedded in methylmethacrylate, and subsequently sectioned by a microtome (Leica, Germany). The sections (5 µm in thickness) were stained with hematoxylin and eosin (H&E, Solarbio, China) and tartrate resistant acid phosphatase (TRAP, Solarbio, China) for histological analysis, and then viewed under an inverted microscope.

ELISA

The serum samples were prepared by centrifugation (2000 × g, 20 min) of the collected blood samples stored at −80 °C until analyzed. Serum concentration of ALP (Nanjing jiancheng, China), IGF-1 (R&D Systems, USA), OPG (ZCI Bio, China), PINP (ZCI Bio, China), RANKL (ZCI Bio, China), and CTX-1 (ZCI Bio, China) was assessed according to the manufacturer's instructions.

Isolation of osteoblasts and osteoclasts, construction of IGF-1 c.258 A > G base edited cells, and Co-culture of osteoblasts and osteoclasts

MC3T3-E1 cells and RAW264.7 cells were purchased from Hycyte biotech (China) cultured in a complete medium containing α-minimum essential medium (α-MEM, Sigma, China), fetal bovine serum (FBS, Gibco, USA), and 1% penicillin/streptomycin (p/s, Solarbio, China) at 37 °C in a humidified atmosphere of 95% air and 5% CO₂ as described previously. MC3T3-E1 was named MC3T3-IGF-1-A. The osteoblast differentiation medium contained 10 mM β-glycerophosphate (Sigma, USA), 50 µg/mL ascorbic acid (Sigma, USA), 10 nmol dexamethasone (Sigma, USA), 10% FBS, and 1% p/s in an α-MEM medium. The osteoclast differentiation medium contained 10% FBS, 1% p/s, 50 ng/ml RANKL (Sino bio, China), and 50 ng/ml M-CSF (Sino bio, China) in an α-MEM medium.

Primary osteoblasts isolation, we followed the protocol previously described by HIROKO SUDO et al.⁴³ with few modifications. Two genotypes of primary osteoblasts were isolated and purified from WT(AA) and Ho(GG) newborn mouse calvaria, named CNCC-IGF-1-A and CNCC-IGF-1-G cells. Cells were cultured in a complete medium at 37 °C in an atmosphere of 5% CO₂. Osteoblast differentiation method as above.

Osteoclast precursors isolation, we followed the protocol previously described by Teun J de Vries et al.⁴⁴ with few modifications. Osteoclast-like cells (OCLs) were flushed from tibia and femurs of three 8-week-old WT(AA) and Ho(GG) male mice, named OCL-IGF-1-A and OCL-IGF-1-G cells. Osteoclast differentiation method as above. Cells were cultured in osteoclast differentiation medium for 7 days to induce OCLs differentiation. OCLs were identified by TRAP staining according to the instructions using a commercial kit (Solarbio, China), and photographed using a microscopy.

IGF-1 c.258 A > G base-edited cell generation was done as previously described. Briefly, site-directed mutagenesis of the mouse IGF-1 was performed by the adenine base-editors (ABEs), two pairs of sgRNAs (sgRNA1: GCATTCGGAGGGACACCTCAG; sgRNA2: GGCACCTCAGACAGGC ATTG) were designed at the corresponding homologous mutation sites to the pig, constructed into pBlueScript II SK (+) (Addgene ID: 74707) vector, and then transfected into MC3T3-E1 cells together with Cas9 vector pCMV-ABEmax (Addgene ID: 112095), obtained after cell sorting, and named MC3T3-IGF-1-G. Cell culture and differentiation were consistent with MC3T3-IGF-1-A.

To evaluate the effect of IGF-1 c.258 A > G synonymous mutation on osteoblast and osteoclast differentiation in a co-culture system, adapted from Alessandra Pinna et al.⁴⁵. CNCCs/MC3T3-E1 cells were separately seeded at an initial density of 5 × 10⁴ cells mL⁻¹ in the bottom chamber of a 6-well transwell plate (0.4 µm pore size, Corning, USA), and cultured with osteoblast differentiation medium for 14 d. Medium was replaced every other day. OCLs and RAW264.7 cells were then respectively seeded at a concentration of 5 × 10⁴ cells mL⁻¹ in the top chamber of the transwell plate to initiate the transwell co-cultures until day 21.

Senescence-associated-β-galactosidase (SA-β-gal) staining

Osteoblasts were treated with 100 µM H₂O₂ (Sigma, USA) for 4 h. The SA-β-gal activity was detected using the in situ β-galactosidase staining kit (Beyotime, China). Cells were seeded into 6-well culture plates at a density of 5 × 10⁵ cells/well, reached 80% confluency, washed three times with PBS, fixed with 4% paraformaldehyde for 15 min, and washed three times with PBS. Next, cells were incubated with the SA-β-gal detection solution overnight at 37 °C without CO₂, washed three times with PBS, and analyzed under an inverted microscope (Nikon, Japan). The experiment was conducted three times.

CCK-8 assay

CCK-8 (Dojindo, Japan) was used to observe cell proliferation. Osteoblasts (5 × 10³ cells/well) were cultured with a complete medium in 96-well plates in triplicate for 24 h. Subsequently, cells were stimulated with 100 µM H₂O₂ for 4 h, cultured for 2, 3, and 4 days, and followed by incubation with 10 µL of the CCK-8 reagent added into each well. A wavelength of 450 nm absorbance was determined by a SpectraMax M5 plate reader (Molecular Devices, USA), which determined the survival rate of the cells.

5-ethynyl-2'-deoxyuridine (EdU) Staining

The EdU Kit (RIBOBIO, China) was assayed the proliferation ability of indicated osteoblasts. The osteoblasts were seeded 5 × 10³ in each 96-well plate. Next, osteoblasts were stimulated with 100 µM H₂O₂ for 4 h, labeled with 50 µM EdU for 4 h, fixed with 4% paraformaldehyde for 30 min, treated with 0.5% Triton-X 100 for 10 min, and incubated for 30 min in a mixture of reagents. The nuclei were stained with DAPI (Solarbio, China) for 5 min. Osteoblasts were then observed under an inverted fluorescence microscope (Nikon, Japan). Three times the experiment was conducted.

Migration assay

The migration activity of osteoblasts in vitro was evaluated by scratch assay. Osteoblasts (5 × 10⁴ cells /well) were cultured in 6-well plates, incubated with 2 mL complete medium overnight, reached confluence, stimulated with 100 µM H₂O₂ for 4 h, and then starved 24 h before scratching. Cells were scraped rapidly, and horizontally in the center of the plate with a pipette tip. Cell migration was photographed under an inverse microscope per 0, 9, and 18 h, and the average width of the scratched gap was measured in triplicate wells by the ImageJ software.

Alkaline phosphatase (ALP) staining and quantification

Osteoblasts were cultured overnight in 24-well plates and 80% confluence after adherence. Then, 100 µM H₂O₂ induced cell senescence for 4 h. Osteoblasts were incubated in an osteoblast differentiation medium containing 10 mM β-glycerophosphate (Sigma, USA), 50 µg/mL ascorbic acid (Sigma, USA), 10 nmol dexamethasone (Sigma, USA), 10% FBS, and 1% p/s in an α-MEM medium for 7 days to increase osteoblast mineralization. The medium was changed every 2–3 days. On day 7, osteoblasts were fixed with 4% polyoxymethylene for 30 min, rinsed thrice in PBS, then incubated in dark at RT for 10–12 h with a mixture of 5-bromo-4-chloro-3-indolyl-phosphate (BCIP) and nitro-blue tetrazolium (NBT) reagents (Beyotime, China), and washed with deionized water for observation under a microscope. Quantification of ALP activity was performed according to the protocols of an ALP activity assay kit (Nanjing Jiancheng, China) and a BCA protein assay kit (Beyotime, China), respectively. Osteoblasts were gently washed three times with PBS, lysed with 0.5% Triton X-100 for 10 min, centrifuged at 12,000 × g for 5 min, and obtained the clear supernatant. ALP activity and protein content were measured in the clear supernatant at wavelengths of 520 and 595 nm using a microplate reader (Molecular Devices, USA). The total protein content was used to adjust ALP activity.

Alizarin red staining (ARS)

Extracellular matrix mineralization capacity is determined by the chelation of alizarin red S (Sigma, USA) with calcium ions to form mineralized nodes. Osteoblasts were seeded 5 × 10⁴ cells/well in 6-well plates, adhesion and

dissemination overnight, and treated with 100 μ M H₂O₂ for 4 h. Then, osteoblasts were cultured for 21 d using an osteoblast differentiation medium (changed every 2–3 day). The cells were rinsed thrice in PBS after medium removal, fixed with 4% formaldehyde for 30 min, rinsed thrice in PBS, and stained with 500 μ L of pH 4.2 and 1% alizarin red stain solution for 30 min. Finally, osteoblasts were washed twice with deionized water and photographed under a microscope. For quantitative analysis, the osteoblasts of stained calcium nodules were incubated with 10% cetylpyridinium chloride (Sigma, USA) per well for 30 min at RT continuous gentle shaking. The extracted stain was transferred to 96-well plates. The optical density value of each well was detected at 562 nm using a microplate reader.

Real-time quantitative PCR (qRT-PCR)

Total RNA from osteoblasts, osteoclasts, and the distal metaphyses of right tibia were isolated with a total RNA extraction kit, according to the protocol of manufacturer (Omega, USA), and quantified the purity and concentration of RNA by NanoDrop 2000 (Thermo, USA). Then, 1 μ g of total RNA was reverse transcribed into cDNA using the PrimeScript RT Reagent Kit with Genomic DNA Eraser (Takara, Japan). 1 μ L of cDNA, 10 μ L of FastStart Universal SYBR Green Master (Roche, USA), 9 μ L Nuclease-free water (Roche, USA), and 0.5 μ L of each forward and reverse specific primers (Comate, China) was used for quantitative real-time PCR in an ABI PRISM

7900HT thermocycler (Applied Biosystems, USA), normalizing with housekeeping gene (GAPDH), and using the $2^{-\Delta\Delta Ct}$ method (Table 1).

Co-immunoprecipitation analysis

The osteoblasts were collected and lysed. For the co-immunoprecipitation studies, the lysates were centrifuged for 15 min at 13,000 \times g and the pre-cleared supernatant was subjected overnight immunoprecipitation using the IGFBP-5 (1:100, Santa Cruz, USA) and IGFBP-3 (1:100, Santa Cruz, USA) antibody at 4 $^{\circ}$ C. On the next day, the antigen-antibody complex and the Protein A/G magnetic bead (MCE, USA) were collected after incubation 2 h at 4 $^{\circ}$ C. The collected protein complexes were washed five times with co-immunoprecipitation buffer and eluted by boiling in protein sample buffer under reducing conditions. Sample proteins were then resolved by SDS-PAGE and analyzed by western blot.

Western blot

Cell proteins were isolated in RIPA buffer (Beyotime, China) on ice, determined by BCA assay (Beyotime, China), adjusted to the same using 5 \times SDS-PAGE loading buffer (Solarbio, China), and denatured for 5 min at 100 $^{\circ}$ C to obtain the final protein samples. Protein samples were separated by electrophoresis on 12% SDS-PAGE gels. Then, samples were electro-transferred to 0.22 μ m polyvinylidene fluoride (PVDF) membranes

Table 1 | Primers for qRT-PCR analysis of expression of target genes

| Primers | Sequences (5' \rightarrow 3') | Extension time (s) | Annealing temperature ($^{\circ}$ C) | PCR product (bp) |
|--------------------------------|---|--------------------|---------------------------------------|------------------|
| <i>IGF-1</i> | F: TGGTGGATGCTCTTCAGTTCGT R: TGCTTTTGTAGGCTTCAGTGGG | 30 | 58.5 | 179 |
| <i>IGF-1R</i> | F: TGGACCCCTCGGCCCTCC R: TCACTTGTCATCGTCGTCCTTG | 30 | 58.5 | 250 |
| <i>p16</i> | F: TAGTCCTTCCTACCCCAATTTCC R: TTGGTCCTTAGCCACTCCTTC | 30 | 58.5 | 76 |
| <i>p21</i> | F: CCTGGTGATGTCCGACCTG R: CCATGAGCGCATCGCAATC | 30 | 58.5 | 103 |
| <i>p53</i> | F: CTCTCCCCGCAAAAGAAAAA R: CGGAACATCTCGAAGCGTTTA | 30 | 58.5 | 84 |
| <i>CyclinD1</i> | F: TTTCTTTCCAGAGTCATCAAGTGT R: TGA CTCCAGAAGGGCTTCAA | 30 | 58.5 | 144 |
| <i>PCNA</i> | F: GAAGTTTTCTGCAAGTGAGAG R: CAGGCTCATTCATCTCTATGGT | 30 | 58.5 | 107 |
| <i>CDK4</i> | F: TCAGTGGTGCCAGAGATGG R: GGAAGGCAGAGATTCGCTTA | 30 | 58.5 | 88 |
| <i>OPG</i> | F: ACACTTTCACTCCAATCGTCC R: TGCCCTTTCCGTTGTGTCC | 30 | 58.5 | 240 |
| <i>OCN</i> | F: AGACTCCGGCGCTACCTT R: CTCGTCAACAAGCAGGGTTAG | 30 | 58.5 | 93 |
| <i>RUNX2</i> | F: GAGGGACTATGGCGTCAAACA R: GGATCCCAAAAGAAGCTTTGC | 30 | 58.5 | 70 |
| <i>OSX</i> | F: TCAGCCGCCCGATCTTCCA R: CAATGGGTCCACCGGCCAAG | 30 | 58.5 | 157 |
| <i>ALP</i> | F: CAACAGGGTAGATTCTTTGG R: GGTGAGATCCAGAATGTTCC | 30 | 58.5 | 135 |
| <i>RANKL</i> | F: TCGTGGAACATTAGCATGGA R: CCTCTCCCAATCTGGTTCAA | 30 | 58.5 | 224 |
| <i>TRAP</i> | F: TCCTGGCTCAAAAAGCAGTT R: ACATAGCCCACACCGTTCTC | 30 | 58.5 | 212 |
| <i>NF-κB</i> | F: GAGGTCTCTGGGGGTACCAT R: AAGGCTGCCTGGATCACTTC | 30 | 58.5 | 89 |
| <i>GAPDH</i> | F: TGGCAAAGTGGAGATTGTTGCC R: AAGATGGTGATGGGCTTCCCG | 30 | 58.5 | 156 |

(Millipore, USA) and blocked with 5% skim milk powder (BD, USA) for 1 h at RT. Then, membranes were incubated overnight at 4 °C with appropriate primary antibodies of anti-rabbit IGF-1 (1:2000, Abcam, USA), anti-rabbit IGF-1R (1:2000, Abcam, USA), anti-rabbit IGFBP-5 (1:100, Santa Cruz, USA), anti-rabbit IGFBP-3 (1:100, Santa Cruz, USA) and anti-rabbit β -actin (1:2000, BBI, China), respectively. The next day, membranes were washed with TBST, and incubated with horseradish peroxidase (HRP)-conjugated secondary antibodies (1:2000, BBI, China) for 1 h at RT. Finally, the membranes were visualized and detected by ECL reagent (Beyotime, China) and quantified using ImageJ software (National Institute of Health, USA).

Statistics and reproducibility

Statistical analyses were performed using GraphPad Prism 9. Statistical significance of two groups and multiple groups were calculated using the Tukey's test and ANOVA. Data in Graphs are expressed as mean \pm SD with at least 3 repeat units. The $P < 0.05$ was considered significant (* $P < 0.05$, ** $P < 0.01$, *** $P < 0.001$).

Reporting summary

Further information on research design is available in the Nature Portfolio Reporting Summary linked to this article.

Data availability

All source data underlying the graphs and charts presented in the main figures and the microscopy images and blots images can be accessed via figshare Entrez (Hao, Linlin (2024). IGF-1 c.258 A > G synonymous mutation ameliorates senile osteoporosis. figshare. Figure. <https://doi.org/10.6084/m9.figshare.27948876.v2>)⁴⁶.

Received: 5 March 2024; Accepted: 4 December 2024;

Published online: 19 December 2024

References

- Compston, J. E., McClung, M. R. & Leslie, W. D. Osteoporosis. *Lancet* **393**, 364–376 (2019).
- Foger-Samwald U., Kersch-Schindl, K., Butylina, M. & Pietschmann, P. Age related osteoporosis: targeting cellular senescence. *Int. J. Mol. Sci.* **23**, 2701 (2022).
- Coughlan, T. & Dockery, F. Osteoporosis and fracture risk in older people. *Clin. Med.* **14**, 187–191 (2014).
- Qadir, A. et al. Senile osteoporosis: the involvement of differentiation and senescence of bone marrow stromal cells. *Int. J. Mol. Sci.* **21**, 349 (2020).
- Johnston, C. B. & Dagar, M. Osteoporosis in older adults. *Med. Clin. North Am.* **104**, 873–884 (2020).
- Crane, J. L. & Cao, X. Function of matrix IGF-1 in coupling bone resorption and formation. *J. Mol. Med.* **92**, 107–115 (2014).
- Giustina, A., Mazziotti, G. & Canalis, E. Growth hormone, insulin-like growth factors, and the skeleton. *Endocr. Rev.* **29**, 535–559 (2008).
- Rico-Llanos, G. A., Becerra, J. & Visser, R. Insulin-like growth factor-1 (IGF-1) enhances the osteogenic activity of bone morphogenetic protein-6 (BMP-6) in vitro and in vivo, and together have a stronger osteogenic effect than when IGF-1 is combined with BMP-2. *J. Biomed. Mater. Res. A* **105**, 1867–1875 (2017).
- Wang, Y. M. et al. Insulin-like growth factor-I is essential for embryonic bone development. *Endocrinology* **147**, 4753–4761 (2006).
- He, J., Rosen, C. J., Adams, D. J. & Kream, B. E. Postnatal growth and bone mass in mice with IGF-I haploinsufficiency. *Bone* **38**, 826–835 (2006).
- Wang, Y. et al. Role of IGF-I signaling in regulating osteoclastogenesis. *J. Bone Min. Res.* **21**, 1350–1358 (2006).
- Chen, C. Y. et al. Overexpression of Insulin-Like Growth Factor 1 enhanced the osteogenic capability of aging bone marrow mesenchymal stem cells. *Theranostics* **7**, 1598–1611 (2017).
- Kao, C. C. et al. The decisive case-control study elaborates the null association between ADAMTS5 rs226794 and Osteoarthritis in Asians: a case-control study and meta-analysis. *Genes* **12**, 1916 (2021).
- Cheng, Y. et al. Porcine IGF1 synonymous mutation alter gene expression and protein binding affinity with IGF1R. *Int. J. Biol. Macromol.* **116**, 23–30 (2018).
- Scicchitano, B. M., Rizzuto, E. & Musaro, A. Counteracting muscle wasting in aging and neuromuscular diseases: the critical role of IGF-1. *Aging* **1**, 451–457 (2009).
- Wang, S. Y. et al. A synonymous mutation in IGF-1 impacts the transcription and translation process of gene expression. *Mol. Ther. Nucleic Acids* **26**, 1446–1465 (2021).
- Di Medio, L. & Brandi, M. L. Advances in bone turnover markers. *Adv. Clin. Chem.* **105**, 101–140 (2021).
- Zhong, Y., Li, J., Luo, J. & Chen, F. Advances in bone turnover markers (PINP and CTX) in optimizing anti-resorptive and anabolic therapies against osteoporosis. *Discov. Med.* **32**, 149–154 (2021).
- Cantatore, F. P. & Pipitone, V. Markers of bone turnover: consideration on their clinical application in osteoporosis. *Painman Med.* **41**, 247–251 (1999).
- Matsushita, M. et al. Age-related changes in bone mass in the senescence-accelerated mouse (SAM). SAM-R/3 and SAM-P/6 as new murine models for senile osteoporosis. *Am. J. Pathol.* **125**, 276–283 (1986).
- Azman, K. F. & Zakaria, R. D-Galactose-induced accelerated aging model: an overview. *Biogerontology* **20**, 763–782 (2019).
- Zhang, Y. B., Zhong, Z. M., Hou, G., Jiang, H. & Chen, J. T. Involvement of oxidative stress in age-related bone loss. *J. Surg. Res.* **169**, e37–e42 (2011).
- Srivastava, M. & Deal, C. Osteoporosis in elderly: prevention and treatment. *Clin. Geriatr. Med.* **18**, 529–555 (2002).
- Ilyas, Z. & Camacho, P. M. Rare adverse effects of bisphosphonate therapy. *Curr. Opin. Endocrinol.* **26**, 335–338 (2019).
- Papapetrou, P. D. Bisphosphonate-associated adverse events. *Hormones* **8**, 96–110 (2009).
- Wang, J. et al. Bone marrow-derived IGF-1 orchestrates maintenance and regeneration of the adult skeleton. *Proc. Natl Acad. Sci. USA* **120**, e2203779120 (2023).
- Ozbas, H., Tutgun Onrat, S. & Ozdamar, K. Genetic and environmental factors in human osteoporosis. *Mol. Biol. Rep.* **39**, 11289–11296 (2012).
- Ralston, S. H. & Uitterlinden, A. G. Genetics of osteoporosis. *Endocr. Rev.* **31**, 629–662 (2010).
- Hosoi, T. Genetic aspects of osteoporosis. *J. Bone Min. Metab.* **28**, 601–607 (2010).
- Liu, Y. P. et al. Association of the g.27563G>A osteoprotegerin genetic polymorphism with bone mineral density in Chinese women. *Genet. Mol. Res.* **13**, 3560–3566 (2014).
- Vidal, C., Cachia, A. & Xuereb-Anastasi, A. Effects of a synonymous variant in exon 9 of the CD44 gene on pre-mRNA splicing in a family with osteoporosis. *Bone* **45**, 736–742 (2009).
- Govoni, K. E., Baylink, D. J. & Mohan, S. The multi-functional role of insulin-like growth factor binding proteins in bone. *Pediatr. Nephrol.* **20**, 261–268 (2005).
- Hurley, M. M., Abreu, C. & Hakeda, Y. Basic fibroblast growth factor regulates IGF-I binding proteins in the clonal osteoblastic cell line MC3T3-E1. *J. Bone Min. Res.* **10**, 222–230 (1995).
- Mazziotti, G. et al. Glucocorticoid-induced osteoporosis: pathophysiological role of GH/IGF-I and PTH/VITAMIN D axes, treatment options and guidelines. *Endocrine* **54**, 603–611 (2016).
- Jiang, H. T. et al. IGF-1 reverses the osteogenic inhibitory effect of dexamethasone on BMP9-induced osteogenic differentiation in mouse embryonic fibroblasts via PI3K/AKT/COX-2 pathway. *J. Steroid Biochem. Mol. Biol.* **191**, 105363 (2019).

36. Wang, Y. et al. Alpha-ketoglutarate ameliorates age-related osteoporosis via regulating histone methylations. *Nat. Commun.* **11**, 5596 (2020).
37. Saferding, V. et al. microRNA-146a controls age-related bone loss. *Aging Cell* **19**, e13244 (2020).
38. Liu, H., Yue, X. & Zhang, G. Downregulation of miR-146a inhibits osteoporosis in the jaws of ovariectomized rats by regulating the Wnt/beta-catenin signaling pathway. *Int. J. Mol. Med.* **47**, 1–1 (2021).
39. Seddighi, H., Klein-Nulend, J. & Jin, J. Osteocyte mechanotransduction in orthodontic tooth movement. *Curr. Osteoporos. Rep.* **21**, 731–742 (2023).
40. Khosla, S. Minireview: the OPG/RANKL/RANK system. *Endocrinology* **142**, 5050–5055 (2001).
41. Vlasi, R., Zhang, X., Wu, M. & Chen, G. Wnt signaling: Essential roles in osteoblast differentiation, bone metabolism and therapeutic implications for bone and skeletal disorders. *Genes Dis.* **10**, 1291–1317 (2023).
42. Nishimura, R., Hata, K. & Kida, J. Regulation of osteoblasts and chondrocytes by Wnt signaling. *Clin. Calcium* **29**, 299–307 (2019).
43. Sudo, H., Kodama, H. A., Amagai, Y., Yamamoto, S. & Kasai, S. In vitro differentiation and calcification in a new clonal osteogenic cell line derived from newborn mouse calvaria. *J. Cell Biol.* **96**, 191–198 (1983).
44. Cao, Y. et al. IL-1beta differently stimulates proliferation and multinucleation of distinct mouse bone marrow osteoclast precursor subsets. *J. Leukoc. Biol.* **100**, 513–523 (2016).
45. Pinna, A. et al. Nanoceria provides antioxidant and osteogenic properties to mesoporous silica nanoparticles for osteoporosis treatment. *Acta Biomater.* **122**, 365–376 (2021).
46. Hao, Linlin. IGF-1 c.258 A > G synonymous mutation ameliorates senile osteoporosis. figshare. Figure. <https://doi.org/10.6084/m9.figshare.27948876.v2> (2024).

Acknowledgements

This work was supported by the National Natural Science Foundation of China (32072813) and the Science and Technology Research and Planning Project of the Education Department of Jilin Province (JJKH20231240KJ), the Bethune Project of Jilin University (2024B39).

Author contributions

Zhaoguo Wang constructed the senile osteoporosis model, IGF-1 c.258 A > G base edited cells and wrote the paper. Dayou Dai isolated the osteoblasts and osteoclasts and co-culture the osteoblasts and osteoclasts. Siyao Wang performed the histomorphometry and elisa experiments. Libo Zhang performed the senescence-associated- β -galactosidase (SA- β -gal) staining, alkaline phosphatase (ALP) staining and alizarin red staining

(ARS). Yi Li conducted the CCK-8, 5-ethynyl-2'-deoxyuridine (EdU) staining and migration assay. Xunming Zhang performed the RT-qPCR and western blot assays. Yunyun Cheng analyzed the data. Linlin Hao conceived and designed the experiments.

Competing interests

The authors declare no competing interests.

Additional information

Supplementary information The online version contains supplementary material available at <https://doi.org/10.1038/s42003-024-07369-x>.

Correspondence and requests for materials should be addressed to Yunyun Cheng or Linlin Hao.

Peer review information *Communications Biology* thanks Shu-Zhang Guo, Daniela Greere, and the other, anonymous, reviewers for their contribution to the peer review of this work. Primary Handling Editors: Martina Rauner and JOao Valente. A peer review file is available.

Reprints and permissions information is available at <http://www.nature.com/reprints>

Publisher's note Springer Nature remains neutral with regard to jurisdictional claims in published maps and institutional affiliations.

Open Access This article is licensed under a Creative Commons Attribution-NonCommercial-NoDerivatives 4.0 International License, which permits any non-commercial use, sharing, distribution and reproduction in any medium or format, as long as you give appropriate credit to the original author(s) and the source, provide a link to the Creative Commons licence, and indicate if you modified the licensed material. You do not have permission under this licence to share adapted material derived from this article or parts of it. The images or other third party material in this article are included in the article's Creative Commons licence, unless indicated otherwise in a credit line to the material. If material is not included in the article's Creative Commons licence and your intended use is not permitted by statutory regulation or exceeds the permitted use, you will need to obtain permission directly from the copyright holder. To view a copy of this licence, visit <http://creativecommons.org/licenses/by-nc-nd/4.0/>.

© The Author(s) 2024